ACS Photonics

Article

pubs.acs.org/journal/apchd5

Three-Dimensional Single Gyroid Photonic Crystals with a Mid-Infrared Bandgap

Siying Peng,[†] Runyu Zhang,[‡] Valerian H. Chen,[†] Emil T. Khabiboulline,[†] Paul Braun,[‡] and Harry A. Atwater*[,†]

[†]Applied Physics, California Institute of Technology, Pasadena, California 91125, United States

[‡]Department of Materials Science and Engineering, University of Illinois at Urbana−Champaign, Champaign, Illinois 61820, United States

Supporting Information

ABSTRACT: A gyroid structure is a distinct morphology that is triply periodic and consists of minimal isosurfaces containing no straight lines. We have designed and synthesized amorphous silicon (a-Si) mid-infrared gyroid photonic crystals that exhibit a complete bandgap in infrared spectroscopy measurements. Photonic crystals were synthesized by deposition of a-Si/Al_2O_3 coatings onto a sacrificial polymer scaffold defined by two-photon lithography. We observed a 100% reflectance at 7.5 μm for single gyroids with a unit cell size of 4.5 μm, in agreement with the photonic bandgap position predicted from full-wave electromagnetic simulations, whereas the observed reflection peak shifted to 8 μm for a 5.5 μm unit cell size. This approach represents a simulation-fabrication-characterization platform to realize three-dimensional gyroid photonic crystals with well-defined dimensions in real space and tailored properties in momentum space.

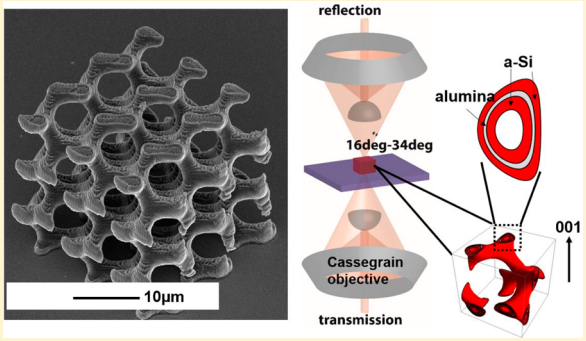

KEYWORDS: *photonic bandgap, three-dimensional photonic crystals, mid-infrared, gyroids, Weyl points*

Three-dimensional photonic crystals offer opportunities to probe interesting photonic states such as bandgaps,[1−8] Weyl points,[9,10] well-controlled dislocations and defects.[11−13] Combinations of morphologies and dielectric constants of materials can be used to achieve desired photonic states. Gyroid crystals have interesting three-dimensional morphologies defined as triply periodic body centered cubic crystals with minimal surfaces containing no straight lines.[9,10,14−19] A single gyroid structure, such as the one shown in Figure 1a, consists of isosurfaces described by

$$\sin(x)\cos(y) + \sin(y)\cos(z) + \sin(z)\cos(x) > u(x, y, z)$$

where the surface is constrained by $u(x,y,z)$. Gyroid structures exist in biological systems in nature. For example, self-organizing process of biological membranes forms gyroid photonic crystals that exhibit the iridescent colors of butterfly's wings.[20] Optical properties of gyroids could vary with tuning of $u(x,y,z)$,[21] unit cell size, and spatial symmetry,[9] as well as refractive index contrast. Single gyroid photonic crystals, when designed with high refractive index and fill fraction, are predicted to possess among the widest complete three-dimensional bandgaps,[9,22] making them interesting for potential device applications such as broadband filters and optical cavities. In this work, we demonstrate a synthesis approach for forming mid-infrared three-dimensional gyroid photonic crystals, and report experimental measurements of the bandgap for a single gyroid structure at mid-infrared wavelengths.

RESULTS

To realize gyroid photonic crystals at mid-infrared wavelengths, we utilize full-wave finite-difference time-domain (FDTD) simulations to determine the dimensions and materials required for crystal design (see Methods). The simulation shown in Figure 1c reveals that a-Si single gyroid crystals with a unit cell size of 5 μm and $u(x,y,z) = 1.1$ (see Table S1 for fill fraction) has a complete bandgap (indicated by the dashed box) from 8 to 10 μm in all symmetry directions of the bcc Brillouin zone in Figure 1b. In units of normalized frequency calculated by dividing unit cell size (a) by wavelength (λ), the complete bandgap is between 0.5 and 0.6. For constant refractive index at mid-infrared wavelength, we can use the value of normalized frequency to deduce bandgap position for crystals with different unit cell size. For example, for a = 5.5 μm single gyroid crystal investigated in Figure 4b, the center of the bandgap can be inferred by a normalized frequency, resulting in a shift of the bandgap center by 0.6 μm. Therefore, we identified a-Si as a suitable material with its high refractive index and low loss at mid-infrared wavelength. Another suitable candidate material is

Received: April 20, 2016
Published: May 23, 2016

DOI: 10.1021/acsphotonics.6b00293
ACS Photonics 2016, 3, 1131−1137

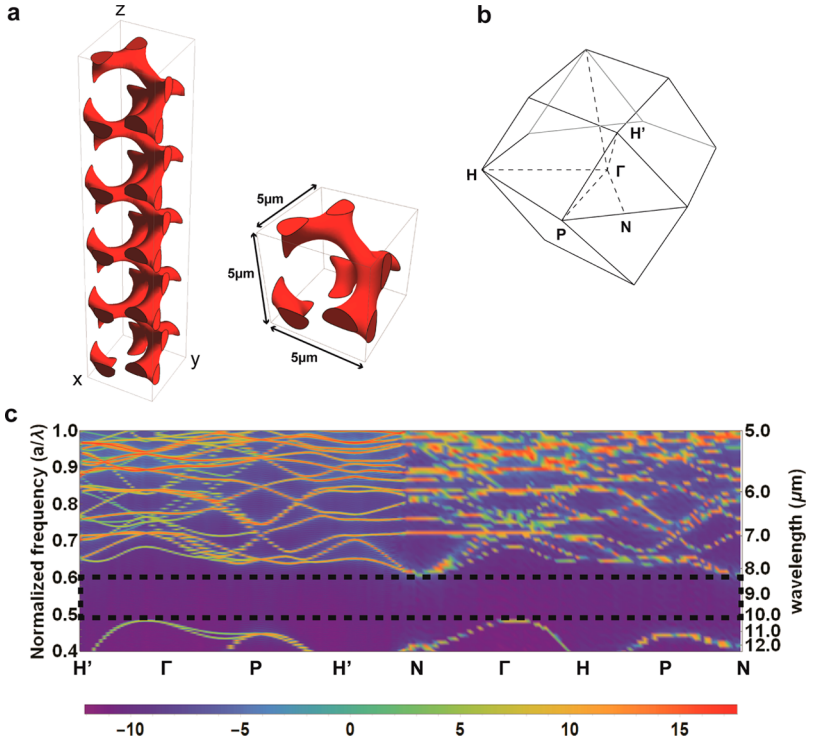

Figure 1. Single gyroid structure and photonic bandstructure simulation. (a) Stacks of unit cells of single gyroid structure. (b) bcc Brillouin zone. (c) Photonic band structure of a-Si single gyroid from full wave simulations, with unit cell size of 5 μm in x, y, and z directions. The color map is proportional to logarithm of the density of states.

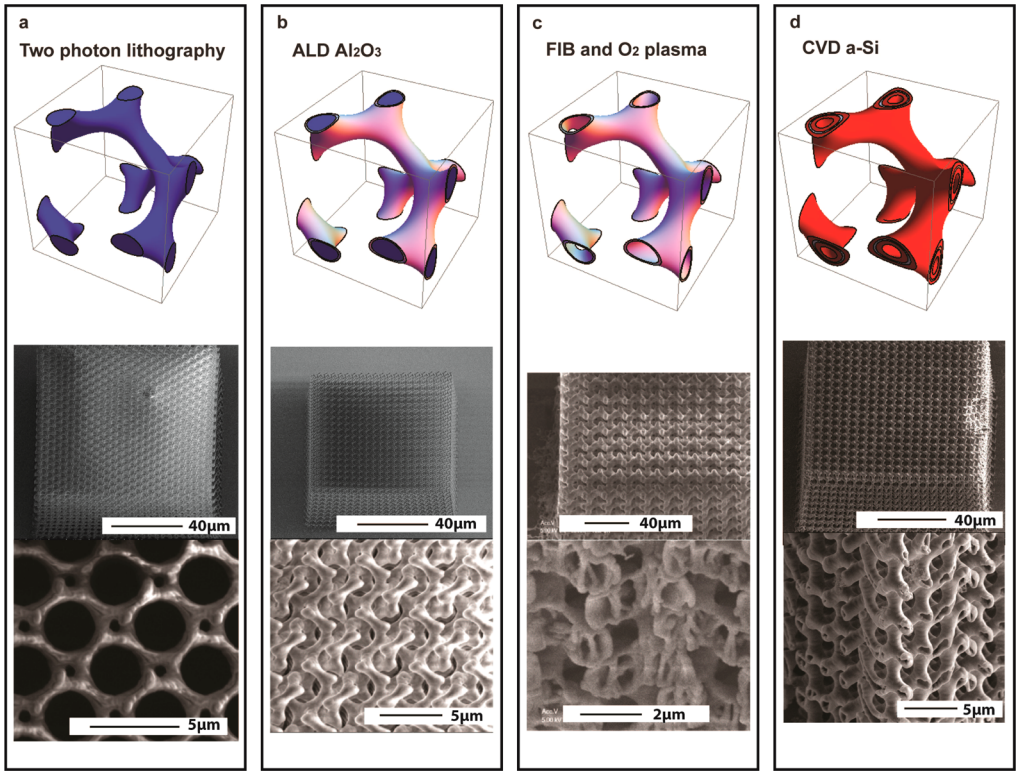

Figure 2. Fabrication procedures of gyroid photonic crystals. (a) Two-photon lithography to define a sacrificial polymer scaffold of the gyroid structure. (b) Atomic layer deposition of Al_2O_3 to coat the polymer structure. (c) Focused ion beam milling to remove the sides of the structure, followed by oxygen plasma to remove the polymer, leaving a hollow alumina structure. (d) Chemical vapor deposition of a-Si to coat and in-fill the hollow alumina structure.

germanium, which has even higher refractive index ($n > 4$) and sufficiently low loss in this wavelength regime.

To fabricate a-Si single gyroid structures, we developed a protocol which incorporates multiple steps[2,12,13,23,24] (see

DOI: 10.1021/acsphotonics.6b00293
ACS Photonics 2016, 3, 1131−1137

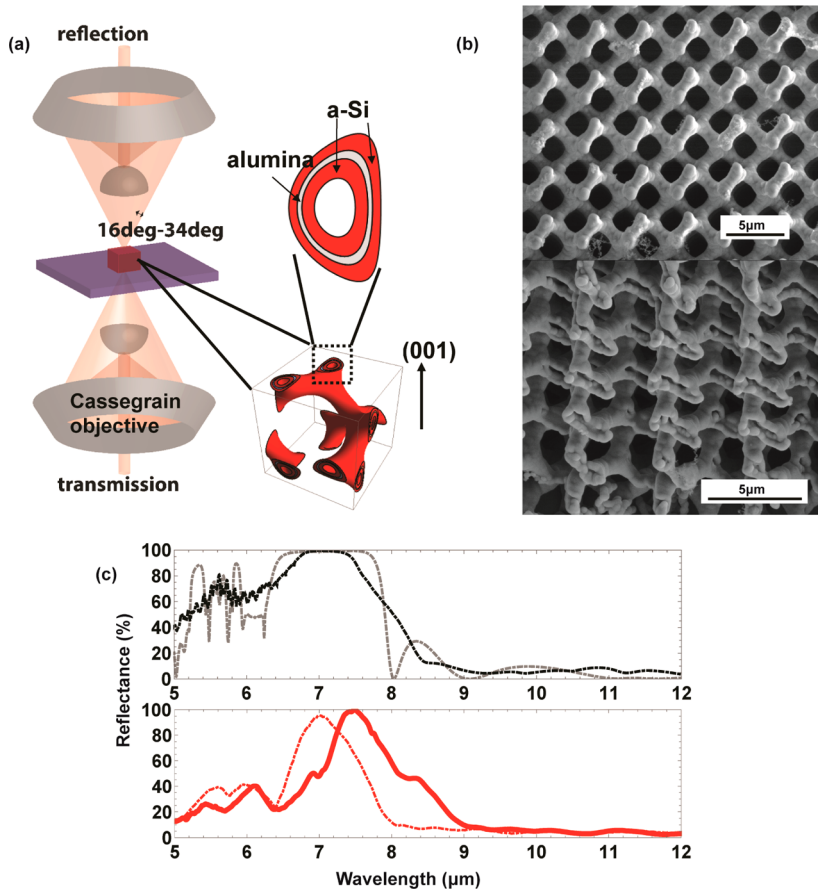

Figure 3. FTIR characterization of bandgaps. (a) Fourier transform infrared spectroscopy experimental configuration. (b) SEM images of a hollow gyroid at (001) crystal orientation with a-Si (150 nm)/Al_2O_3 (40 nm)/a-Si (150 nm) layers. (c) Reflectance spectrum from full wave simulations of a hollow gyroid at (001) crystal orientation with a-Si (100 nm)/Al_2O_3 (40 nm)/a-Si (100 nm) layers (gray dashed line), reflectance spectrum from full wave simulations of a trapezoidal hollow gyroid at (001) crystal orientation with a-Si (100 nm)/Al_2O_3 (40 nm)/a-Si (100 nm) layers (black dashed line), FTIR measurement of a hollow gyroid with a-Si (100 nm)/Al_2O_3 (40 nm)/a-Si (100 nm) layers (red dashed line) and FTIR measurement of a hollow gyroid with a-Si (150 nm)/Al_2O_3 (40 nm)/a-Si (150 nm) layers (red dashed line).

Methods for detailed description), as illustrated in Figure 2. Two-photon lithography was utilized to directly write a sacrificial polymer scaffold of gyroid photonic crystals with unit cell sizes of 4.5, 5.1, and 5.5 μm on mid-infrared transparent silicon substrates. Each sample is composed of 20 × 20 × 10 unit cells. We conformally deposited 40 nm thick aluminum oxide coatings on the polymer gyroids via atomic layer deposition (ALD) at 150 °C. We then used focused ion beam (FIB) milling to remove the crystal sides to facilitate polymer removal, yielding a hollow inorganic aluminum oxide crystal after oxygen plasma cleaning. Subsequently, the structure was conformally coated and in-filled with a 100 nm a-Si layer at 350 °C using chemical vapor deposition (CVD). The polymer structure is not structurally stable at temperatures above 250 °C, which are typically necessary for conformal deposition of high refractive index materials such as a-Si. Therefore, the hollow aluminum oxide crystal is a critical intermediate structure to provide a scaffold that can withstand high temperature. The final structure consists of a 40 nm middle layer of aluminum oxide and two 100 nm/150 nm a-Si layers on both the inside and outside of the aluminum oxide scaffold, corresponding to $u(x,y,z)$ values of 1.1/1.05, 1.2, 1.25, and 1.35/1.37 for coated a-Si, Al_2O_3, in-filled a-Si and inner hollow part, respectively (see Table S1 for fill fraction values).

We characterized the resulting a-Si single gyroid photonic crystals by Fourier transform infrared spectroscopy (FTIR), shown in Figure 3a (see Methods for a detailed description of the measurements). SEM images of the characterized sample are shown in Figure 3b. The reflectance spectrum of the a = 4.5 μm sample reveals a peak of 98% at 7.0 μm, as shown in Figure 3c (red dashed line), in agreement with the predicted reflectance peak center of the 4.5 μm trapezoidal structure in the figure above (black dashed line; see the section of Full Wave Simulation on Deformed Crystals in Methods), as well as the band gap center for a cubical single gyroid structure (gray dashed line). The reflectance of the sample is normalized to the reflectance of an atomically smooth gold mirror of 97% reflectance. Additional 50 nm coating and in-filling of a-Si on the structure red-shifted the reflectance peak to 7.5 μm, giving rise to the 100% reflectance peak shown in Figure 3c (red solid line). The reflectance peak at 7.5 μm is a direct manifestation of a photonic bandgap. The transmittance spectrum shown in Figure 4a has a wide 0% transmittance band centered at 7.5 μm, confirming the bandgap. The extinction (scattering + absorption) is obtained by subtracting the transmittance and reflectance percentages from 100%. Since the FTIR collection angle is limited to 16−34°, that part of the reflected light that lies outside of this angular range is considered as scattering here. These results reveal the photonic property of the single

DOI: 10.1021/acsphotonics.6b00293
ACS Photonics 2016, 3, 1131−1137

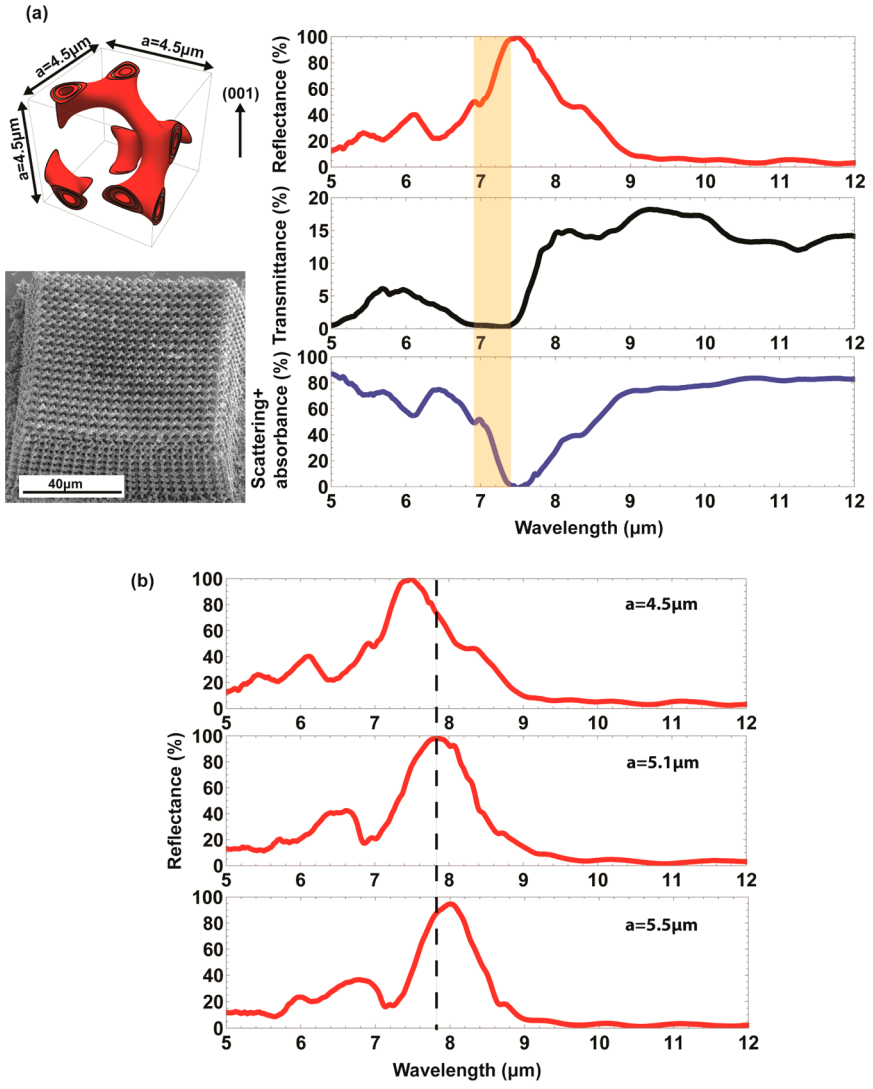

Figure 4. FTIR characterization of single gyroids. (a) Reflectance, transmittance, and scattering + absorbance from a single gyroid structure with unit cell size of 4.5 μm and a total of 20 × 20 × 10 cells. (b) Comparison of reflection spectra of samples with unit cell sizes of 4.5, 5.1, and 5.5 μm (20 × 20 × 10 unit cells).

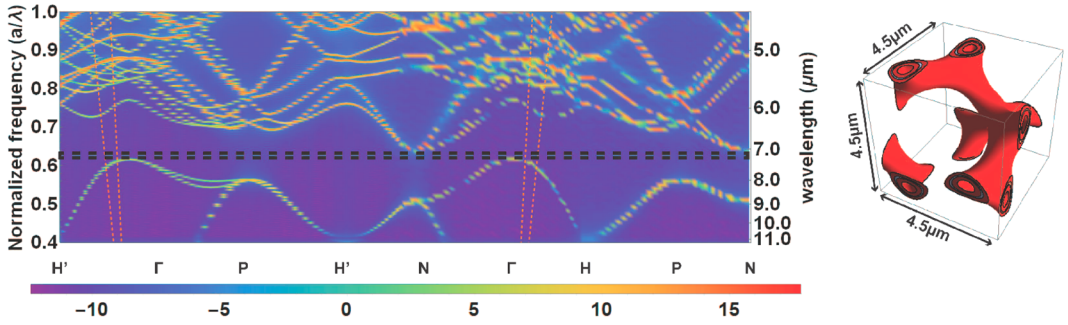

Figure 5. Photonic band structure simulation. Photonic band structure of a single gyroid consists of a-Si (100 nm)/Al_2O_3 (40 nm)/a-Si (100 nm) layers from full wave simulations, with unit cell size of 4.5 μm in x, y, and z directions. Bands in between the orange lines are accessible through FTIR characterization shown in Figure 3a.

gyroid structure, namely, the optical bandgap in the mid-infrared regime.

We also characterized the reflectance spectrum of the a = 5.1 μm period and a = 5.5 μm period samples and compared them with that of the a = 4.5 μm sample, as shown in Figure 4b. We observed a red shift of the reflection peaks by 0.6 μm in wavelength for the 5.5 μm period sample, and a shift of 0.4 μm in the 5.1 μm sample relative to the 4.5 μm sample, which is in agreement with the increase in the bandgap wavelength predicted (see Figures 1c and 5). This observation can be intuitively understood by considering the resonant coupling between the incoming beam and the cavity of a periodic unit

DOI: 10.1021/acsphotonics.6b00293
ACS Photonics 2016, 3, 1131−1137

cell. The agreement between our experimental results and simulations for three structures with different unit cell sizes confirms the mid-infrared bandgap feature of the single gyroid photonic crystals.

DISCUSSION

Several specific features arise in the reflectance spectra of these single gyroid samples due to practical aspects of the chosen material compositions and defects present in the crystal structures. The bandgap center of the 4.5 μm period structure is shifted from the predicted 8 μm wavelength inferred from Figures 1c and 3c (black dashed line) to the experimentally measured 7.0 μm wavelength in Figure 3c (red dashed line). This is due to lower effective refractive index of the a-Si/Al_2O_3/a-Si heterostructure present in fabricated samples as compared with an assumed homogeneous dense solid a-Si cross-section for the photonic crystal elements in the simulations given in Figure 1c. The center of the bandgap calculated from full wave simulation for the actual a-Si (100 nm)/Al_2O_3 (40 nm)/a-Si (100 nm) composition is at 7 μm, shown in Figure 5. Another minor contribution comes from the lower refractive index in the experimental a-Si as compared to those of Palik[25] used in full wave simulations, shown in Figure S1a, likely due to differences in the deposition conditions.

The main crystal defect is a overall shape distortion of the lattice which is attributed to polymer shrinkage, as shown in SEM images in Figures 2 and 4, instead of the cubic shape expected in an ideal lattice. A trapezoidally shaped crystal is formed as the result of the polymer scaffold shrinkage. After direct laser writing, the written IP-Dip photoresist cross-links to form polymer scaffolds. The unwritten photoresist is then removed in the process of development, during which the top portion of the polymer scaffold shrinks. The adhesion force between the scaffold and the rigid Si substrate prevents the bottom lattice from shrinking. This distortion results in a decreasing unit cell size from the bottom to the top of the crystal, resulting in an overall trapezoidal shape for the crystal. In an ideal cubic crystal, we expect a 100% reflectance peak with bandwidth matching that of the predicted bandgap, shown in Figure 3c (black dashed line). A narrowing of the measured reflectance peak in Figure 3c (red dashed line) is expected when the trapezoidal shape is taken into account in the deformed crystal simulation (see Methods, Full Wave Simulation on Deformed Crystals), together with the a-Si/Al_2O_3/a-Si material composition. Intuitively, the measured reflectance spectrum is a superposition of the scattering from each crystal layer over the range of momenta accessible by the 16° to 34° range of incident angles of the FTIR configuration shown in Figures 3a and 5 (orange lines). As the unit cell dimension increases from top to bottom of the trapezoidal shaped crystal, the reflectance peak center of each layer is increasingly red-shifted. The width of the measured reflectance narrows as a result of the effective inhomogeneity and the lowered effective refractive index. The second reflectance peak observed in Figure 4b, at 6.1 μm for the a = 4.5 μm sample, 6.5 μm for the a = 5.1 μm sample, and 6.8 μm for the a = 5.5 μm sample, respectively, can also be explained by this effective inhomogeneity. From reflectance simulations of an ideal a-Si gyroid crystal in Figure 3c (gray dashed line), distinct photonic bands exist above the band gap, manifested as sharp dips in the reflectance spectrum. The states observed in the reflectance spectra is equivalent of projected band structure on the (001) plane, spanned by Γ-H and Γ-H′ symmetry directions. Band structure simulations in Figures 1c and 5 indicate photonic bands above the band gap. A trapezoidal shaped crystal gives rise to spectral inhomogeneity, and consequently the photonic band features broadens into one reflectance peak. Despite realistic material compositions and sample defects, the essential physics interpreted from these reflectance spectra is not affected by the above-mentioned nonidealities.

CONCLUSION

In conclusion, we experimentally observed a 100% reflective bandgap at mid-infrared wavelengths in single gyroid photonic crystals with high refractive index materials, fabricated using two-photon lithography and conformal layer deposition, confirming photonic bandgap predictions obtained from simulations. This mid-infrared bandgap is also predictably tunable by changing the unit cell size in the simulation design and fabrication. The synthesis/characterization approach described here opens the door to design of more complex mid-infrared photonic crystals with topological states, such as Weyl points in double gyroid photonic crystal with parity-breaking symmetry, for which synthesis of single gyroid photonic crystals establishes feasibility. Further designs may also yield gyroid photonic structures whose surfaces exhibit topologically protected states, suggesting the possibility to synthesize these intriguing structures to create unusual states and phases of light.

METHODS

Full Wave Band Structure Simulation. Simulations were performed using Lumerical FDTD Solutions v8.15.716. In simulations, bands are excited by randomly placing dipoles inside the simulation region that is defined by Bloch boundary conditions in x, y, and z directions. Randomly placed field monitors record electric and magnetic fields over time. Fourier transformation of the overall electric field versus time reveal spectrum of the bands. By tuning phase of the Bloch boundary conditions, we were able to calculate bands at wave vectors along all high symmetry directions in the Brillouin zone of a bcc lattice. Palik[25] n, k data for a-Si are used in the simulation (shown in Supporting Information, Figure 1S).

Sample Fabrication. Polymer gyroid structures were written in negative photoresist IP-Dip using the Photonic Professional GT system (Nanoscribe GmbH). The 40 nm thick aluminum oxide coatings on the polymer gyroids were conformally deposited via atomic layer deposition at 150 °C in a Cambridge Nanotech S200 ALD System with H_2O and trimethylaluminum (TMA) precursors. We used focused ion beam milling with the FEI Nova 200 Nanolab at 30 kV and 30 nA Ga beam condition to remove the crystal sides to facilitate polymer removal. We etched out the polymers with oxygen plasma using the March PX-500 plasma etcher, yielding a hollow inorganic aluminum oxide crystal. Then the structure is conformally coated and in-filled with 100 nm/150 nm of a-Si at 350 °C using static chemical vapor deposition, with refilled silane as the precursor at an average deposition speed of 10 nm/hour. Refractive index of both deposited a-Si and Al_2O_3 are measured and shown in Supporting Information, Figure 1S.

FTIR Characterization. The mid-infrared light is incident on the sample at incidence angles from 16° to 34° after being focused with a Cassegrain objective. The sample sits on an intrinsic double side-polished silicon substrate with the (001) crystal surface of the gyroid structure in parallel with the

DOI: 10.1021/acsphotonics.6b00293
ACS Photonics 2016, 3, 1131−1137

substrate surface. Reflection and transmission spectra are collected from the same range of angles with two identical Cassegrain objectives on each side of the sample, respectively. Each incidence angle could excite a corresponding wave vector in a specific symmetry direction in the band structure. For three-dimensional crystal structures, the orientation of the crystal could determine projection of the band structure onto a specific symmetry plane.

Full Wave Simulation on Deformed Crystals. Simulations were performed using Lumerical FDTD Solutions v8.15.716. To take into account effects of polymer shrinkage during the structure developing process, we performed full wave simulation approximating the trapezoidal morphology shown in SEM images in Figures 2 and 4. The simulated structure is infinitely periodic in the x and y directions and has a finite length of three unit cells in the z direction, with the a-Si/Al_2O_3/a-Si material composition. The simulation region has periodic boundary condition in the x and y directions and perfectly matched layer (PML) absorbing boundary condition in the z direction. Plane wave source incidents on the structure in the (001) direction as indicated in Figure 3a. Frequency domain field monitors are placed above and below the structure to collect reflection and transmission spectra. We repeated the simulation for a series of unit cell sizes ranging from 4.2 to 4.7 μm with an increment of 0.1 μm. The arithmetic average of these six reflectance spectra, shown as the black dashed line in Figure 3c, is used to approximate the trapezoidal effect on the reflectance spectrum.

■ ASSOCIATED CONTENT

Supporting Information

The Supporting Information is available free of charge on the ACS Publications website at DOI: 10.1021/acsphotonics.6b00293.

Optical constants of deposited materials (a-Si and Al_2O_3) and $u(x,y,z)$ vs fill fraction (PDF).

■ AUTHOR INFORMATION

Corresponding Author

*E-mail: haa@caltech.edu.

Notes

The authors declare no competing financial interest.

■ ACKNOWLEDGMENTS

This work is part of the Light Material Interactions in Energy Conversion Energy Frontier Research Center funded by the U.S. Department of Energy, Office of Science, Office of Basic Energy Sciences under Award Number DE-SC0001293.The authors thank George Rossman for FT-IR assistance, the Kavli Nanoscience Institute at Caltech for cleanroom facilities, the Lewis Group ALD facility at Caltech, and V. W. Brar and F. Liu for insightful discussions.

■ REFERENCES

(1) Lin, S. Y.; Fleming, J. G.; Hetherington, D. L.; Smith, B. K.; Biswas, R.; Ho, K. M.; Sigalas, M. M.; Zubrzycki, W.; Kurtz, S. R.; Bur, J. A three-dimensional photonic crystal operating at infrared wavelengths. *Nature* **1998**, *394*, 251−253.

(2) García-Santamaría, F.; Xu, M.; Lousse, V.; Fan, S.; Braun, P. V.; Lewis, J. A. A Germanium Inverse Woodpile Structure with a Large Photonic Band Gap. *Adv. Mater.* **2007**, *19*, 1567−1570.

(3) Wijnhoven, J. E. G. J.; Vos, W. L. Preparation of Photonic Crystals Made of Air Spheres in Titania. *Science* **1998**, *281*, 802−804.

(4) Vlasov, Y. A.; Bo, X.-Z.; Sturm, J. C.; Norris, D. J. On-chip natural assembly of silicon photonic bandgap crystals. *Nature* **2001**, *414*, 289−293.

(5) Noda, S.; Tomoda, K.; Yamamoto, N.; Chutinan, A. Full Three-Dimensional Photonic Bandgap Crystals at Near-Infrared Wavelengths. *Science* **2000**, *289*, 604−606.

(6) Blanco, A.; Chomski, E.; Grabtchak, S.; Ibisate, M.; John, S.; Leonard, S. W.; Lopez, C.; Meseguer, F.; Miguez, H.; Mondia, J. P.; Ozin, G. A.; Toader, O.; van Driel, H. M. Large-scale synthesis of a silicon photonic crystal with a complete three-dimensional bandgap near 1.5 micrometres. *Nature* **2000**, *405*, 437−440.

(7) Deubel, M.; von Freymann, G.; Wegener, M.; Pereira, S.; Busch, K.; Soukoulis, C. M. Direct laser writing of three-dimensional photonic-crystal templates for telecommunications. *Nat. Mater.* **2004**, *3*, 444−447.

(8) Fleming, J. G.; Lin, S. Y.; El-Kady, I.; Biswas, R.; Ho, K. M. All-metallic three-dimensional photonic crystals with a large infrared bandgap. *Nature* **2002**, *417*, 52−55.

(9) Lu, L.; Fu, L.; Joannopoulos, J. D.; Soljacic, M. Weyl points and line nodes in gyroid photonic crystals. *Nat. Photonics* **2013**, *7*, 294−299.

(10) Lu, L.; Wang, Z. Y.; Ye, D. X.; Ran, L. X.; Fu, L.; Joannopoulos, J. D.; Soljacic, M. TOPOLOGICAL MATTER Experimental observation of Weyl points. *Science* **2015**, *349*, 622−624.

(11) Qi, M.; Lidorikis, E.; Rakich, P. T.; Johnson, S. G.; Joannopoulos, J. D.; Ippen, E. P.; Smith, H. I. A three-dimensional optical photonic crystal with designed point defects. *Nature* **2004**, *429*, 538−542.

(12) Ramanan, V.; Nelson, E.; Brzezinski, A.; Braun, P. V.; Wiltzius, P. Three dimensional silicon-air photonic crystals with controlled defects using interference lithography. *Appl. Phys. Lett.* **2008**, *92*, 173304.

(13) Rinne, S. A.; Garcia-Santamaria, F.; Braun, P. V. Embedded cavities and waveguides in three-dimensional silicon photonic crystals. *Nat. Photonics* **2008**, *2*, 52−56.

(14) Dolan, J. A.; Wilts, B. D.; Vignolini, S.; Baumberg, J. J.; Steiner, U.; Wilkinson, T. D. Optical Properties of Gyroid Structured Materials: From Photonic Crystals to Metamaterials. *Adv. Opt. Mater.* **2015**, *3*, 12−32.

(15) Prayakarao, S.; Robbins, S.; Kinsey, N.; Boltasseva, A.; Shalaev, V. M.; Wiesner, U. B.; Bonner, C. E.; Hussain, R.; Noginova, N.; Noginov, M. A. Gyroidal titanium nitride as nonmetallic metamaterial. *Opt. Mater. Express* **2015**, *5*, 1316−1322.

(16) Thiel, M.; Rill, M. S.; von Freymann, G.; Wegener, M. Three-Dimensional Bi-Chiral Photonic Crystals. *Adv. Mater.* **2009**, *21*, 4680−4682.

(17) Turner, M. D.; Saba, M.; Zhang, Q.; Cumming, B. P.; Schroder-Turk, G. E.; Gu, M. Miniature chiral beamsplitter based on gyroid photonic crystals. *Nat. Photonics* **2013**, *7*, 801−805.

(18) Vignolini, S.; Yufa, N. A.; Cunha, P. S.; Guldin, S.; Rushkin, I.; Stefik, M.; Hur, K.; Wiesner, U.; Baumberg, J. J.; Steiner, U. A 3D Optical Metamaterial Made by Self-Assembly. *Adv. Mater.* **2012**, *24*, OP23−OP27.

(19) Turner, M. D.; Schröder-Turk, G. E.; Gu, M. Fabrication and characterization of three-dimensional biomimetic chiral composites. *Opt. Express* **2011**, *19*, 10001−10008.

(20) Saranathan, V.; Osuji, C. O.; Mochrie, S. G. J.; Noh, H.; Narayanan, S.; Sandy, A.; Dufresne, E. R.; Prum, R. O. Structure, function, and self-assembly of single network gyroid (I4132) photonic crystals in butterfly wing scales. *Proc. Natl. Acad. Sci. U. S. A.* **2010**, *107*, 11676−11681.

(21) Babin, V.; Garstecki, P.; Hołyst, R. Photonic properties of multicontinuous cubic phases. *Phys. Rev. B: Condens. Matter Mater. Phys.* **2002**, *66*, 235120.

(22) Cumming, B. P.; Turner, M. D.; Schröder-Turk, G. E.; Debbarma, S.; Luther-Davies, B.; Gu, M. Adaptive optics enhanced

DOI: 10.1021/acsphotonics.6b00293
ACS Photonics 2016, 3, 1131−1137

direct laser writing of high refractive index gyroid photonic crystals in chalcogenide glass. *Opt. Express* **2014**, *22*, 689−698.
(23) Gratson, G. M.; García-Santamaría, F.; Lousse, V.; Xu, M.; Fan, S.; Lewis, J. A.; Braun, P. V. Direct-Write Assembly of Three-Dimensional Photonic Crystals: Conversion of Polymer Scaffolds to Silicon Hollow-Woodpile Structures. *Adv. Mater.* **2006**, *18*, 461−465.
(24) Moon, J. H.; Xu, Y.; Dan, Y.; Yang, S. M.; Johnson, A. T.; Yang, S. Triply Periodic Bicontinuous Structures as Templates for Photonic Crystals: A Pinch-off Problem. *Adv. Mater.* **2007**, *19*, 1510−1514.
(25) Piller, H. Silicon (Amorphous) (a-Si). In *Handbook of Optical Constants of Solids*; Palik, E. D., Ed.; Academic Press: Burlington, 1997; pp 571−586.

DOI: 10.1021/acsphotonics.6b00293
ACS Photonics 2016, 3, 1131−1137